

Anomalous divergence of a relaxation time in discontinuous shear thickening suspensions

Rijan Maharjan and Eric Brown

Department of Mechanical Engineering and Materials Science, Yale University, New Haven, CT 06520

(Dated: June 14, 2022)

We investigated the transient relaxation of a Discontinuous Shear Thickening (DST) suspension of cornstarch in water. Starting from a steady shear in a parallel plate rheometer, we stopped the top plate rotation and measured the transient stress relaxation. We found that at low effective packing fraction ϕ_{eff} , the suspensions exhibited a relaxation behavior consistent with a rheometric fluid in which the relaxation is determined by the steady-state viscosity. However, for larger ϕ_{eff} , we find up to two exponential relaxation regimes, which both become distinct from the rheometric model. The discrepancy between the measured relaxation times and the rheometric prediction was found to be as large as 4 orders of magnitude and diverges in the limit as $\phi_{eff} \rightarrow \phi_c$, corresponding to the liquid solid transition, as the measured relaxation times diverge to infinity while the rheometric prediction approaches 0. In this limit, the measured relaxation time scales are on the order of ~ 1 s, which may be important to understanding the dynamic phenomenon exhibited by DST suspensions. We also showed that using the shear rate $\dot{\gamma}_c$ at the onset of shear thickening to characterize the effective packing fraction ϕ_{eff} can more precisely characterize material properties near ϕ_c . This conversion to ϕ_{eff} can also be used to compare experiments done in other laboratories or under different temperature and humidity conditions on a consistent ϕ_{eff} scale at our reference temperature and humidity environment.

PACS numbers: 47.50.-d, 83.60.Rs, 47.57.E-, 83.80.Hj

Discontinuous Shear Thickening (DST) suspensions are known for exhibiting several transient and dynamic phenomena, including an unusually strong impact response – strong enough to be used in commercial impact protection devices [11, 13], the ability of people to run on the surface of cornstarch and water [4, 25], and a shear resistance strong enough to break or jam industrial mixing equipment [1]. Our goal is to characterize the transient relaxation component of the rheology of DST suspensions to ultimately understand such phenomena.

Traditionally, shear thickening is defined by an increase in effective viscosity η with increasing shear rate $\dot{\gamma}$ or shear stress τ , where $\eta = \tau/\dot{\gamma}$ in a steady state flow in a rheometer. In many concentrated suspensions such as cornstarch and water, this effect can be so strong that the increase of η or τ in $\dot{\gamma}$ can be 1-3 orders of magnitude, and can even appear to be discontinuous in $\dot{\gamma}$ at a critical shear rate $\dot{\gamma}_c$. The steepness of $\tau(\dot{\gamma})$ tends to increase with packing fraction up to a critical point at packing fraction ϕ_c (corresponding to the liquid-solid transition), above which shear thickening is no longer observed [5, 6], so shear thickening is most prominent just below ϕ_c (see [1, 4, 23] for reviews on shear thickening).

Transient impact experiments have revealed a very different rheology than the steady-state $\tau(\dot{\gamma})$ from rheometer experiments described in the previous paragraph. For example, under impact the suspensions support stresses orders of magnitude larger than inferred from steady-state rheometer measurements [18, 24]. This contradicts the standard viewpoint of rheology that assumes fluids are rheometric – meaning the same viscosity function $\tau(\dot{\gamma})$ that has a single value of τ at each $\dot{\gamma}$ is a constitutive relation that could describe flow under differ-

ent conditions (i.e. geometries, boundary conditions, and transients).

Another remarkable phenomena of DST fluids is the formation of stable holes in the surface of a vertically vibrated layer of the fluid [16]. It has been shown that these structures cannot be stable due to a rheology described by any rheometric function of the form $\tau(\dot{\gamma})$ – regardless of whether the function includes shear thickening. Instead the $\tau(\dot{\gamma})$ must have a hysteresis such that there is a difference in stress on the up- and down-cycles of the vibration to overcome the gravitational and surface tension forces that are trying to close the hole [7]. A third unusual observation in DST fluids is that a sphere sinking in the fluid will have an oscillating velocity, rather than monotonically approaching a terminal velocity [21]. It was shown that this also cannot be described with any rheometric function $\tau(\dot{\gamma})$, rather it can also be described in principle by hysteresis in $\tau(\dot{\gamma})$ [21, 22].

Making use of this knowledge that hysteresis in $\tau(\dot{\gamma})$ is required to explain transient and dynamic phenomena of DST fluids, a simple phenomenological model was proposed by Ozgen et al. [19]. It consisted of a $\tau(\dot{\gamma})$ relationship with an effective viscosity that increases with shear rate to mimic shear thickening. This term was made to have hysteresis in $\tau(\dot{\gamma})$ so that it depends not only on the instantaneous shear rate, but on a weighted average of shear rate over a preceding time interval (corresponding physically to a time delayed response), as well as a relaxation time over which the viscosity decays after the shear decreases. This model was able to qualitatively reproduce the phenomena that were previously argued to require hysteresis; the stable holes in a vibrated layer, and oscillations in the velocity of a sinking sphere. The

model also reproduced some phenomena that are known to occur in DST fluids, but have not been explained previously; in particular the abilities of a sphere to bounce and roll on the surface of the suspension [26]. This success is remarkable in that no simulation has been able to produce any one of these phenomenon before even separately, yet several were produced at once with this model. However, this model was made before the any of the relevant rheological parameters were measured for real materials, so the parameters were freely tuned to reproduce these phenomena.

Despite the interest in these transient and dynamic phenomena, it is remarkable that there has been little systematic study of transient rheology or any rheology outside of the traditional $\tau(\dot{\gamma})$ relation for DST suspensions. While a relaxation of stress to a steady-state behavior has been observed previously [14], analysis of this transient, or any trends in control parameters such as packing fraction, have not been reported. Oscillatory rheology is often used to characterize time-dependent rheology, from which it has been found that there is also a minimum strain amplitude required for shear thickening in addition to the critical shear rate [12, 20], but in general these results supported the steady shear rheology description, and no indication of any transient effects or a characteristic time scale independent from the critical shear rate was reported. Thus, even if we make use of oscillatory rheology we do not have a rheometric constitutive model that can capture the transient and dynamic behavior of DST fluids.

To characterize the relaxation behavior, in this paper we report measurements of the relaxation of stress after a flow is stopped, as a function of packing fraction near the liquid-solid transition where shear thickening behavior is strongest and exhibits the most dramatic transitions [5, 6]. It is expected that this relaxation data will be an essential element in constitutive models of transient and dynamic phenomena such as proposed by Ozgen et al. [19]. The other time-dependent behavior required for the hysteresis – a delay in stress response after impact – is reported in another paper [18].

The remainder of this paper is organized as follows. We describe the materials and methods used in Secs. I and II, respectively. In Sec. III we show typical steady-state viscosity curves from which we draw parameter values to compare to transient measurements. In Sec. IV we present a method to more precisely characterize the effective packing fraction near the liquid-solid transition, which turns out to be helpful for resolving trends in relaxation behavior in this limit. In Sec. V, we report measurements of the relaxation of stress over time after a flow is stopped to obtain a relaxation time, and show that it is inconsistent with predictions from steady-state rheology in the limit of high packing fractions.

I. MATERIALS

Cornstarch was purchased from *Carolina Biological Supply* and suspended in tap water to use as a typical DST fluid [4]. The samples were created at 22.0 ± 0.6 °C and humidity of $48 \pm 6\%$, where the uncertainties represent day-to-day variations in the respective values. A four-point scale was used to measure quantities of cornstarch and water to obtain a packing fraction ϕ by weight. While using packing fraction by volume is more traditional, obtaining the packing fraction by volume requires knowing the water content (which depends on temperature and humidity) and porosity of the cornstarch – both of which are difficult to obtain [4]. The effective uncertainty in the packing fraction is 0.7% due to the adsorption of water by cornstarch.

The suspension was mixed until no dry powder was observed. The sample was further shaken in a *Scientific Instruments Vortex Genie 2* for 30 seconds to 1 minute on approximately 60% of its maximum power output. We directly measured a density of 1200 ± 20 kg/m³ for a suspension at $\phi = 0.57$ based on the volume and weight in a graduated cylinder. If we extrapolate based on the fraction of cornstarch and water using the known density of water, this same value is consistent with the density for suspensions within the uncertainty for packing fractions from 0.51 to 0.63, covering our entire measurement range.

II. METHODS

The suspension was measured in an *Anton Paar MCR 302* rheometer in a parallel plate setup. The rheometer measured the torque M on the top plate which we controlled to rotate at a constant angular velocity ω . The mean shear stress is given by $\tau = 2M/\pi R^3$ where $R = 25.00$ mm is the radius of the plate. The mean shear rate at the edge of the plate is given by $\dot{\gamma} = R\omega/d$ where $d = 1.250$ mm is the gap height between the plates unless otherwise noted. The viscosity of the sample is measured as $\eta = \tau/\dot{\gamma}$ in a steady state. The sample radius was 25.0 ± 0.5 mm, which corresponds to an 8% error in the stress measurements. The experiments were performed at a plate temperature of 23.5 ± 0.4 °C. A solvent trap was used to slow down the moisture exchange between the sample and the atmosphere. The solvent trap effectively placed a water seal around the sample, with a lipped lid around the sample and the lips touching a small amount of water contained on the top, cupped, surface of the tool.

The sample was pre-sheared to produce a state independent of the sample loading history. We used a linear ramp in shear rate over 200 seconds, covering a shear rate range that crosses the shear thickening regime and a net shear strain greater than 100%. The shear rate was then ramped down and back up twice with a constant rate of variation on a logarithmic scale, with 10 data points per decade and data averaged for 50 seconds per point.

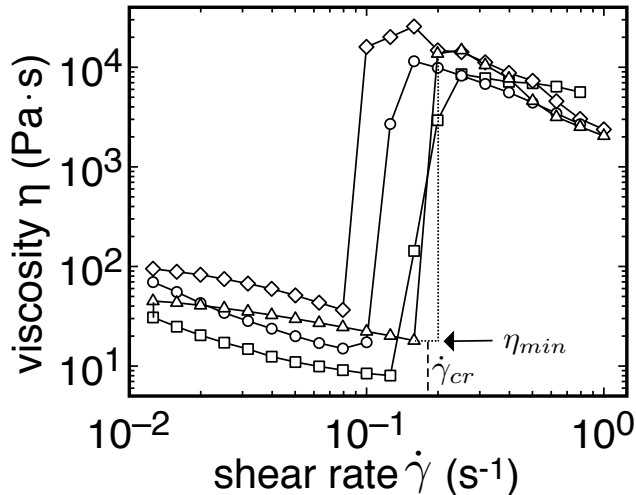


FIG. 1: A typical set of viscosity η vs. shear rate $\dot{\gamma}$ curves for cornstarch and water at packing fraction $\phi = 59.6\%$. The critical shear rate $\dot{\gamma}_c$ and minimum viscosity η_{min} are obtained at the onset of shear thickening. The symbols correspond to different ramps of increasing $\dot{\gamma}$ (squares, diamonds) and decreasing $\dot{\gamma}$ (triangles, circles).

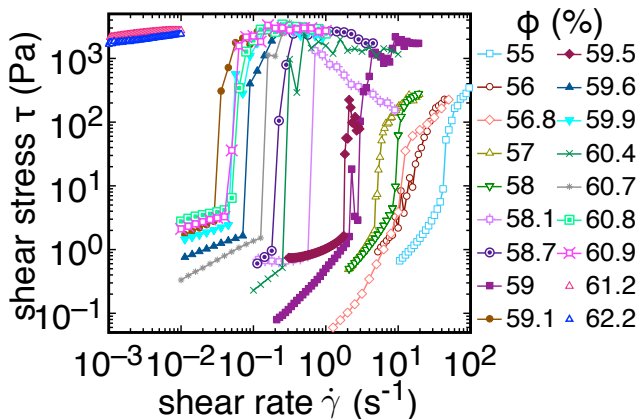


FIG. 2: Shear stress τ as a function of shear rate $\dot{\gamma}$ at different packing fractions ϕ shown in the key. In each case for $\phi < \phi_c = 61.0\%$, DST is seen as a sharp jump in stress, from τ_{min} ($\sim 10^0$ Pa) and τ_{max} ($\sim 10^3$ Pa). For $\phi > \phi_c$, a yield stress of $\sim 10^3$ Pa is observed instead of shear thickening.

III. STEADY STATE VISCOSITY CURVES

Figure 1 shows an example of the steady state viscosity η as a function of shear rate $\dot{\gamma}$ for the four ramps after the preshear at $\phi = 59.6\%$. There is a large run-to-run variation; the standard deviation of the 4 ramps is 30%. We observed no systematic trend from the 1st to 2nd pair of ramps, confirming the pre-shear eliminated any effect of loading history.

Averages of the shear stress τ as a function of shear rate $\dot{\gamma}$ over the 4 ramps are shown in Fig. 2 for different packing fractions ϕ . At each packing fraction, a dis-

continuous jump in $\tau(\dot{\gamma})$ is observed, corresponding to DST. Typically, higher packing fractions have lower critical shear rates $\dot{\gamma}_c$ but there are some exceptions to this due to the uncertainty in packing fraction measured directly. These observations are quite typical of DST suspensions [1, 4, 23] – we present them here for comparison to relaxation measurements later.

At higher packing fractions $\phi > 61.0\%$, we observed a large yield stress as seen in Fig. 2. We identified the liquid-solid transition $\phi_c = 61.0 \pm 0.7\%$, also called the jamming transition, as the packing fraction where there is a sharp transition in the yield stress up to the scale of 10^3 Pa [5]. We did not observe shear thickening at packing fractions above ϕ_c because of the large yield stress [5, 6]. In all of these cases presented, the Reynolds Number $Re = \rho d^2 \dot{\gamma} / \eta < 1$ over the entire shear thickening range. Hence, inertia should not play a role in any of our steady-state measurements.

IV. CHARACTERIZING A MORE PRECISE EFFECTIVE PACKING FRACTION NEAR THE CRITICAL POINT

For a rheometric fluid, the relaxation time would be expected to scale with the viscosity η , which diverges as it approaches the critical point at packing fraction ϕ_c [5, 6]. In testing whether the relaxation time scales with the viscosity as in a rheometric fluid, there is a resolution limit due to the uncertainty in the packing fraction of 1-2%, due to the variability of the packing fraction with temperature and humidity because cornstarch adsorbs water from the atmosphere [8]. This can lead to large changes in the measured viscosity in repetitions of experiments from day-to-day, with infinite sensitivity due to the divergence of the viscosity at a nearby critical packing fraction ϕ_c [5, 6]. For example, in Fig. 2, we see up to an order of magnitude decrease in $\dot{\gamma}_c$ when the apparent packing fraction decreases by 0.5% (counter to the typical trend) when ϕ is within 1% of ϕ_c .

This resolution limit can be circumvented, and scalings tested closer to the critical point by instead characterizing the material in terms of a measurable property that diverges at ϕ_c . Two such properties include the minimum viscosity η_{min} and the inverse of the critical shear rate $\dot{\gamma}_c^{-1}$, both at the onset (i.e. minimum shear rate) of the shear thickening range [5]. Thus, in order to obtain a more reliable measure of effective packing fraction near the critical point, we measure these values for each ϕ to use as references for an effective packing fraction ϕ_{eff} that is more accurate in identifying the sample than ϕ .

We identify a critical shear rate $\dot{\gamma}_c$ and viscosity at the onset of shear thickening η_{min} from the viscosity curves in Fig. 2. We averaged $\dot{\gamma}$ over the point just before and the point just after the jump shown in Fig. 1 for each ramp, then averaged over the 4 ramps to obtain a best estimate of the critical shear rate $\dot{\gamma}_c$. The viscosity at the lower end of the shear thickening range η_{min} was obtained by

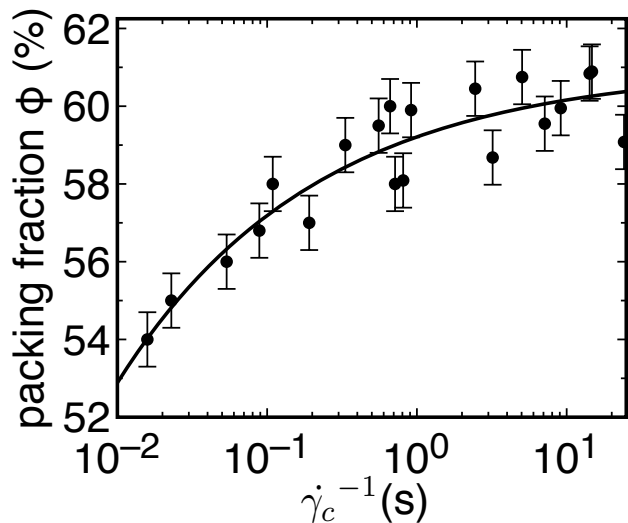


FIG. 3: Directly measured packing fraction ϕ as function of inverse critical shear rate $\dot{\gamma}_c^{-1}$. A fit yields a conversion function $\phi_{eff} = -1.8\% \dot{\gamma}_c^{0.33} + 61.0\%$, which can be used to identify an effective packing fraction ϕ_{eff} based on the measured physical parameter $\dot{\gamma}_c$, which is useful for precise characterizations near the critical packing fraction $\phi_c = 61.0\%$.

averaging the η value just before the jump over the four ramps. For both $\dot{\gamma}_c$ and η_{min} we report the uncertainty as the standard deviation of the mean of the values from the four ramps, which are on average 16% for $\dot{\gamma}_c$ and and 30% for η .

To obtain a conversion to effective packing fraction ϕ_{eff} , we plot the directly measured ϕ as a function of $\dot{\gamma}_c^{-1}$ for data at different packing fractions ϕ in Fig. 3. The conversion is obtained by fitting a power law $\phi_{eff} = A \dot{\gamma}_c^B + \phi_c$ to the data with fixed $\phi_c = 61.0\%$ and fit parameters A and B . If we adjust errors to 0.7% (corresponding to the typical uncertainty in ϕ before the conversion) to obtain a reduced $\chi^2 \approx 1$, the fit yields $A = -1.8 \pm 0.2$ and $B = 0.33 \pm 0.03$, corresponding to the conversion function

$$\phi_{eff} = -1.8\% \dot{\gamma}_c^{0.33} + 61.0\% . \quad (1)$$

If we instead additionally fit the value of ϕ_c , then we obtained $\phi_c = 60.8 \pm 0.6$, consistent with the value obtained from yield stress measurements for the same data set [5].

With this conversion function, we can now calculate an effective packing fraction ϕ_{eff} from a measured $\dot{\gamma}_c$, where the ϕ_{eff} corresponds to the value of the packing fraction in our reference temperature and humidity environment. This conversion can be used for experiments done in other laboratories or under different temperature and humidity conditions to compare different measurements on the same ϕ_{eff} scale, something which has not been successfully done before due to the sensitivity of the packing fraction of suspensions like cornstarch and water to temperature and humidity.

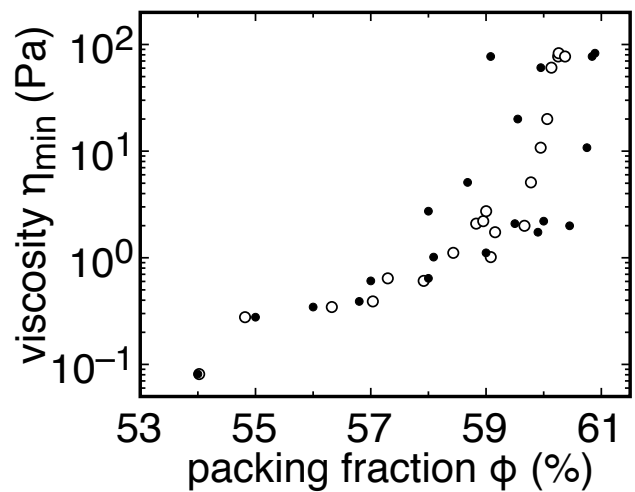


FIG. 4: Onset viscosity η_{min} . Solid symbols: as a function of the directly measured packing fraction ϕ . Open symbols: as a function of the effective packing fraction ϕ_{eff} obtained from the fit of $\dot{\gamma}_c^{-1}$ in Fig. 3. Using the effective packing fraction ϕ_{eff} results in less scatter, allowing a clearer characterization of the trend in measured parameters near the critical point.

To test the usefulness of this effective packing fraction ϕ_{eff} , values of the onset viscosity η_{min} from the same data in Fig. 3 are plotted in Fig. 4 for different directly measured packing fractions ϕ . Near ϕ_c , the data is very scattered as expected due to the error on the x-axis, making it difficult to track the expected divergence in packing fraction. For comparison, values of η_{min} are plotted in the same figure as a function of ϕ_{eff} using Eq. 1 to get ϕ_{eff} from the measured $\dot{\gamma}_c$ at each packing fraction. It can be seen that there is much less scatter in the data in terms of effective packing fraction ϕ_{eff} near ϕ_c , confirming that the fit of Eq. 1 more precisely relates to mechanical properties that diverge near ϕ_c (i.e. η_{min} , $\dot{\gamma}_c^{-1}$) than direct packing fraction ϕ measurements.

V. RELAXATION TIME

To measure the relaxation time, we performed a transient experiment where we first rotated the tool at a shear rate $\dot{\gamma}$ about 60% higher than the critical shear rate $\dot{\gamma}_c$ to achieve a steady-state in the stress at a value above the maximum stress τ_{max} of the shear thickening range (i.e. in the high viscosity shear thinning regime seen in Fig. 1). After a steady-state was reached, we set the tool to a constant shear rate $\dot{\gamma} = 0$, and measured the relaxation of the stress on the tool over time due to the relaxation of the fluid. Figure 5 shows an example of both the control (shear rate) and the response (shear stress) as a function of time for a sample with $\phi_{eff} = 59.7\%$ ($\dot{\gamma}_c^{-1} = 2.4$ s). The tool started rotating at a fixed shear rate of $\dot{\gamma} = 0.7$ s⁻¹, after which the shear stress τ reached a steady value of $\sim 10^3$ Pa. At time $t = 0$ s, we set $\dot{\gamma} = 0$. An expo-

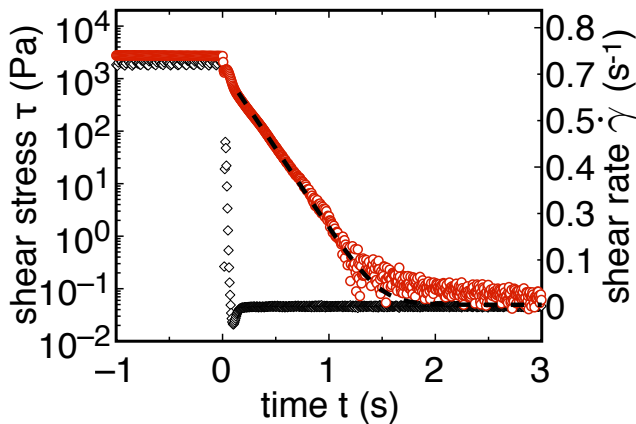


FIG. 5: An example of a transient experiment used to measure a relaxation time. Open diamonds: the controlled shear rate $\dot{\gamma}$, which was first set to a constant shear rate $\dot{\gamma} = 0.7 \text{ s}^{-1}$ up until time $t = 0 \text{ s}$, then held at $\dot{\gamma} = 0 \text{ s}^{-1}$ (right axis scale). Open circles: measured shear stress τ response (left axis scale). Dashed line: exponential fit of Eq. 2 to obtain the relaxation timescale T_1 .

nential relaxation in the stress over time is observed in Fig. 5

To define a relaxation timescale T_1 , we fit the measured $\tau(t)$ during the relaxation to the exponentially decaying function

$$\tau \propto \exp(-t/T_1) + \text{constant} . \quad (2)$$

An example fit is shown in Fig. 5. To avoid a contribution from the acceleration of the tool immediately after the shear rate was set to zero, we started fitting after $\dot{\gamma}$ was less than 5% of its set point value at $t < 0$. The data was fit from that point onwards to the end of the experiment. The input error on the fit was adjusted until the reduced $\chi^2 \approx 1$ to obtain an error on the fit value of T_1 assuming the exponential is a good fit function. The resulting fit captures the relaxation behavior quite well.

While the exponential function provides a good fit to the data in Fig. 5 and other cases at low ϕ , at higher ϕ the stress relaxation appears to have two exponential regimes, as shown for example in Fig. 6 for example at $\phi_{eff} = 60.1\%$ ($\dot{\gamma}_c^{-1} = 9.1 \text{ s}$). To describe this we use the fit function

$$\tau \propto \left(\frac{1}{\exp(-t/T_1)} + \frac{1}{\exp(-t/T_2)} \right)^{-1} + \text{constant} \quad (3)$$

where T_1 and T_2 are two relaxation time scales we can obtain from the data. We fit this to the data in Fig. 6 in two steps to provide better fit stability. The first step fits Eq. 2 to the data the same way as in Fig. 5 to fit the earlier, slower relaxation. After T_1 is determined from this fit, we fit Eq. 3 to the data with only T_2 as a free parameter, and only to the range $\tau \leq 10 \text{ Pa}$, with the same error fitting technique.

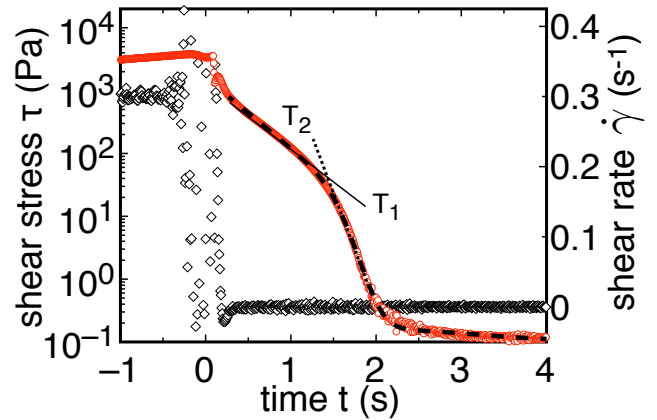


FIG. 6: An example of a transient experiment similar to Fig. 5, however in this case two exponential scaling regimes found. Open diamonds: the controlled shear rate $\dot{\gamma}$ (right axis scale). Open circles: measured shear stress τ response (left axis scale). Dashed line: exponential fit of Eq. 3 to obtain the relaxation timescales T_1 (dotted line) and T_2 (solid line).

A. Relaxation times as a function of packing fraction

To compare the different relaxation behavior, Fig. 7a shows examples of the stress relaxation $\tau(t)$ for all effective packing fractions ϕ_{eff} . The dual-exponential relaxation shown in Fig. 6 is found for $\phi_{eff} \geq 59.8\%$ ($\dot{\gamma}_c^{-1} \geq 3.2 \text{ s}$), while a single exponential relaxation is found for lower ϕ_{eff} . When two exponential ranges can be fit, the transition between the two exponential scaling regimes always happens on the scale of $\tau \sim 10^2 \text{ Pa}$. This stress scale does not correspond to any stress scale known from steady-state rheology. It is in between the two known stress scales: $\tau_{min} \sim 10^0 \text{ Pa}$ at the lower end of the shear thickening regime and $\tau_{max} \sim 10^3 \text{ Pa}$ at the upper end of the shear thickening regime as seen in Fig. 2 [5, 8]. The constant stress value reached in the limit of large time in each case is consistent with the yield stress measured from the steady-state measurements in Fig. 2.

For $\phi < 58.2\%$ ($\dot{\gamma}_c^{-1} \leq 0.26 \text{ s}$), there are some qualitative differences from the behavior shown in Fig. 5 for $58.2\% < \phi_{eff} < 59.8\%$, even though they both exhibit a single exponential relaxation. We show a zoomed in version of panel a in panel b of Fig. 7 to see these differences more closely. For $\phi < 58.2\%$ ($\dot{\gamma}_c^{-1} \leq 0.26 \text{ s}$), extrapolations of the fits of Eq. 2 shown in Fig. 7b fall well below the stress at $t = 0$, indicating that there is an initial relaxation regime that is faster than what we can resolve (limited by the instrument relaxation to its steady state). As a result, we are only able to resolve the behavior that begins at lower stress $\tau \leq \tau_{min} \sim 10^0 \text{ Pa}$, more than an order of magnitude below the stress at $t = 0$. In these cases, the steady state stress for $t < 0$ also only reached a lower magnitude $\sim 10^2 \text{ Pa}$, in contrast with $\phi_{eff} > 58.2\%$ where the steady state stress

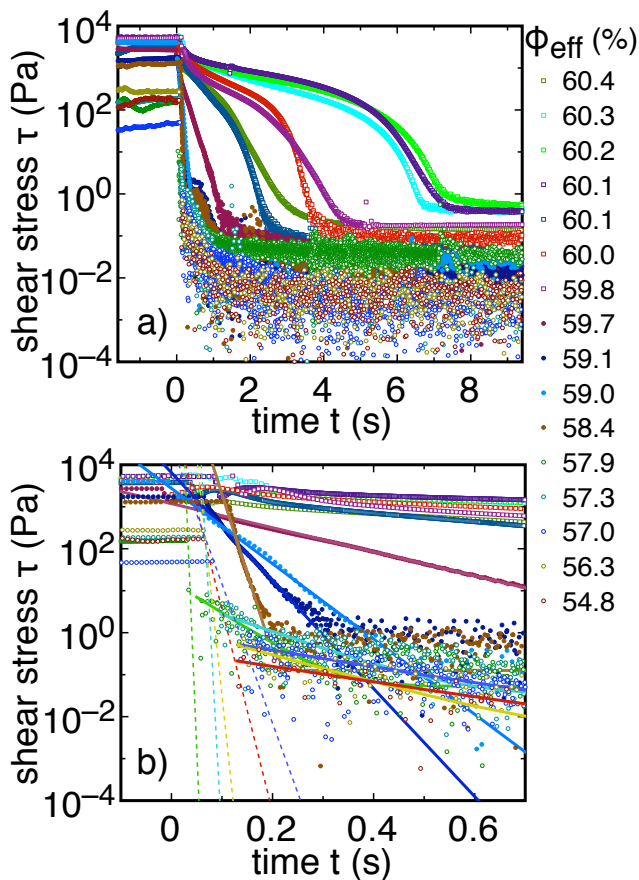


FIG. 7: Relaxation of stress τ over time t for different packing fractions ϕ_{eff} (listed in the legend). (a) Dual-exponential relaxation is found for $\phi_{eff} \geq 59.8\%$ (open squares), while single exponential relaxation is fit for lower ϕ_{eff} (circles). (b) Zoomed scale of panel a to show there is a quicker relaxation behavior that we cannot resolve for $\phi_{eff} < 58.2\%$ (open circles). For $58.2 \leq \phi_{eff} < 59.8\%$ the relaxation follows a single exponential (solid circles). Solid lines: fits of Eq. 2 to the samples with single exponential behavior. Dashed lines: upper limit of the fast, early relaxation behavior based on the rheometric model of Eq. 5 using the maximum viscosity of the shear thickening range η_{max} , showing the fast relaxation we cannot resolve is at least consistent with the rheometric model.

was $\sim 10^3$ Pa.

The relaxation time scales T_1 and T_2 are shown as a function of the onset shear rate $\dot{\gamma}_c^{-1}$ in Fig. 8, where $\dot{\gamma}_c^{-1}$ is a proxy for the packing fraction, but with much higher resolution as ϕ approaches ϕ_c since it diverges in that limit. Errors were obtained from the fits of Eq. 2 and 3 by forcing the reduced $\chi^2 \approx 1$, which were small compared to the standard deviation of the mean of multiple (typically 5) repetitions, so the latter error is plotted. When two separate relaxation times are found for $\phi_{eff} \geq 59.8\%$ ($\dot{\gamma}_c^{-1} > 3.2$ s), they start to deviate from each other. In the limit of $\dot{\gamma}_c^{-1} \rightarrow \infty$, corresponding to the liquid-solid transition as $\phi \rightarrow \phi_c$ [5], an extrapolation of T_1 appears

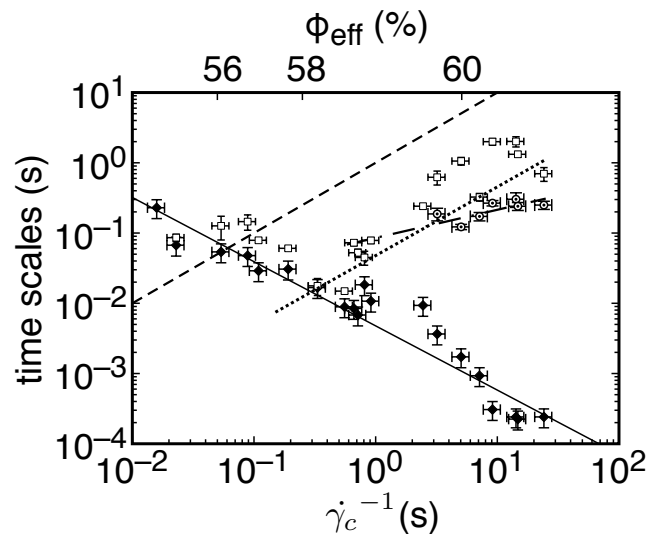


FIG. 8: Relaxation timescales as a function of inverse critical shear rate $\dot{\gamma}_c^{-1}$, which is a proxy for the packing fraction. The top x-axis scale shows some corresponding values of ϕ_{eff} (not a linear scale) for reference. Open squares: the first relaxation time T_1 . Circles with dots in the center: the second relaxation time T_2 . Solid diamonds: rheometric model prediction T_N , which agrees with T_1 for $\phi_{eff} < 58.2\%$ ($\dot{\gamma}_c^{-1} < 0.26$ s). Solid line: power law fit of T_N . Dotted line: power law fit to T_1 for the range it deviates from the rheometric model. Long dashed line: power law fit to T_2 . The measured relaxation timescales T_1 and T_2 both deviate from the rheometric model T_N by several orders of magnitude and diverge to infinity in the limit of large $\dot{\gamma}_c^{-1}$, corresponding to $\phi \rightarrow \phi_c$ (the liquid-solid transition). Dashed line: the timescale corresponding to the inverse critical shear rate $\dot{\gamma}_c^{-1}$, which has a similar scaling as T_1 .

to diverge to infinity, as indicated by the dotted line fit with slope 1.0 ± 0.1 as a guide to the eye. T_2 appears to have a slight positive slope of 0.4 ± 0.2 (long dashed line) and an extrapolation may also diverge to infinity in the same limit, but much more slowly than T_1 .

B. Comparison to relaxation of a Newtonian fluid

Now that we have identified the existence of the relaxation time, we can compare it to the behavior of a rheometric fluid in which the viscosity function $\eta(\dot{\gamma})$ is expected to predict the relaxation behavior in a transient flow. First, we start with a simpler model for a Newtonian fluid, in which the viscosity η is constant. In a transient flow, the torque M on the tool is expected to balance the moment of inertia $I = \pi \rho R^4 d / 2$ times the angular acceleration $\dot{\omega}$. Since $\dot{\omega}$ is not uniform in the fluid, we present equations for a characteristic $\dot{\omega}$ at the edge of the top plate, but this makes the relationships only true as scaling relationships. We will later make them exact by calibrating with a Newtonian fluid. The torque can be related to the viscosity by $M = \eta \omega \pi R^4 / 2d$ for a

rheometric fluid [17] to obtain the differential equation of motion

$$I\dot{\omega} \propto M = -\frac{\eta\omega\pi R^4}{2d} \quad (4)$$

This equation has the solution of an exponential decay for ω , and since the stress $\tau \propto M \propto \omega$ for a Newtonian fluid, then the solution for the stress is also an exponential decay, consistent with what is shown in Fig. 5. The corresponding timescale of the exponential decay can be obtained from Eq. 4 to be proportional to

$$T_N \propto \left| \frac{\omega}{\dot{\omega}} \right| = \frac{\rho d^2}{\eta} . \quad (5)$$

To calibrate the coefficient in Eq. 5, we use a Newtonian fluid of known viscosity (light mineral oil $\eta = 0.054$ Pa·s at 22°C, $\rho = 830$ kg/m³). The relaxation time matches Eq. 5 if we insert the proportionality coefficient 9.9; thus we have the relationship

$$T_N = \frac{9.9\rho d^2}{\eta} \quad (6)$$

for a Newtonian fluid.

To compare this prediction to data in Fig. 8, we use the viscosity at the onset of shear thickening η_{min} for the value of η in Eq. 6 as a best characterization of a single value of a hydrodynamic viscosity for a DST fluid [4]. This is shown as solid diamonds in Fig. 8. The solid line is a power law fit of T_N , which yields an exponent -0.92 ± 0.05 , consistent within 2 standard deviations of the known inverse scaling between onset viscosity η_{min} ($\propto T_N^{-1}$) and onset shear rate $\dot{\gamma}_c$ [5].

The prediction T_N agrees well with the measured relaxation time T_1 for $\phi_{eff} < 58.2\%$ ($\dot{\gamma}_c^{-1} < 0.26$ s). This works because in these experiments the stress range of the fit is below τ_{min} where the viscosity is very close to η_{min} (as seen in Fig. 1) which was used in the calculation of T_N . However, this only describes part of the relaxation seen in Fig. 7b, as at smaller times there is a much faster relaxation that we could not resolve before the tool stopped accelerating. To get an idea of whether this has to do with the higher viscosity at the upper end of the shear thickening range, which is where the experiment starts, a prediction for T_N using the maximum viscosity in the shear thickening range η_{max} is plotted as dashed lines in Fig. 7b for each packing fraction. This acts as an upper bound on the predicted stress for rheometric model, as the viscosity is always less than η_{max} . This prediction is always above the data, so the relaxation behavior is consistent with the predictions of the rheometric model for $\phi_{eff} < 58.2\%$ ($\dot{\gamma}_c^{-1} < 0.26$ s), although a more precise comparison cannot be made due to the fact that we cannot resolve measurements at these short timescales.

At higher packing fractions $\phi_{eff} > 58.2\%$ ($\dot{\gamma}_c^{-1} > 0.26$ s) shown in Fig. 8, the measured T_1 and T_2 deviate significantly from the Newtonian prediction T_N . This deviation becomes as large as 4 orders of magnitude at the highest ϕ_{eff} measured. Extrapolating the trend of T_1 (indicated by the dotted line fit) to the limit of $\dot{\gamma}_c^{-1} \rightarrow \infty$ (corresponding to the liquid-solid transition at $\phi = \phi_c$ [5]) suggests that the T_1 is diverging to infinity in the same limit that the prediction T_N goes to zero. We note that modifying the simple prediction of T_N from Eq. 6 to account for non-Newtonian viscosity function $\tau(\dot{\gamma})$ cannot reduce this discrepancy; since η_{min} is the minimum viscosity in the shear thickening range, the values shown for T_N in Fig. 8 are an *upper* bound on the possible values of T_N over the range of the measured $\eta(\dot{\gamma})$. For a relaxation model with a varying $\tau(\dot{\gamma})$, one would also expect a non-exponential relaxation behavior with a gradually varying slope on a log-linear scale, in disagreement with the observations in Fig. 7.

For comparison, we plot $\dot{\gamma}_c^{-1}$, which is also a timescale, as the short dashed line in Fig. 8. This does not match any of the other time scales plotted, although it is nearly parallel to T_1 . It is possible that in the limit of large packing fraction, T_1 may be determined by $\dot{\gamma}_c$. It was proposed in some early shear thickening models based on hydrodynamic mechanisms that $\dot{\gamma}_c^{-1}$ should be proportional to a relaxation time of the system [3, 10]. However, in this packing fraction range, DST of cornstarch and water is dominated by frictional interactions rather than hydrodynamics [8], and those early hydrodynamic models do not predict the sharp jump in $\tau(\dot{\gamma})$ that defines DST. While they do not provide complete descriptions of DST, it is possible that some elements of those early hydrodynamic models remain relevant to describe the relaxation behavior observed here.

To check if the relaxation behavior is robust, we also performed similar relaxation experiments in a stress controlled system using a couette cell geometry, where we set the stress to 0 after a steady-state stress, and fitted the tool position as a function of time to obtain a relaxation time. We found a qualitatively similar response, for instance, the relaxation time started deviating from the Newtonian model at a packing fraction 3% below ϕ_c and diverged to infinity in the limit of high packing fraction in both cases. The scale of the relaxation time is not directly comparable, as this is expected from the rheometric model to depend on the geometry of the system as well as the mass the tool in a stress-controlled experiment, however we can compare some ratios. In the limit of large ϕ , we found the relaxation time to be up to 5 orders of magnitude higher than the Newtonian model prediction. While this difference is an order of magnitude higher than what we observed in the rate controlled measurements, the precise value depends on how close each experiment was able to get to ϕ_c , so this amount of variation is expected for an uncertainty in ϕ of 0.7%. These observations suggest that the relaxation behavior is robust to different types of flow geometries and driving

conditions.

The divergence of the relaxation time approaching the liquid-solid transition is also reminiscent of a glass transition [9]. It has been established that shear thickening suspensions do exhibit a jamming transition at this same packing fraction [5], which has long been assumed to be similar to a glass transition, but approached from the direction of increasing packing fraction [15]. Melting of a shear-jammed solid state to a liquid state under vibration has also been found to have a diverging relaxation time at the jamming transition in a system that exhibits shear thickening [2]. At this time it is not obvious what the precise connection to the divergent relaxation times in these other systems is or if there is a connection, but the similarities are too many to ignore.

VI. CONCLUSIONS

As part of the process to obtain high resolution measurements near the critical point at the liquid solid transition ϕ_c , we showed that using the critical shear rate $\dot{\gamma}_c$ to characterize an effective packing fraction ϕ_{eff} can more precisely characterize material properties near ϕ_c (Fig. 4). This conversion to ϕ_{eff} (Fig. 3) can also be used to compare experiments done in other laboratories or under different temperature and humidity conditions on a consistent ϕ_{eff} scale at our reference temperature and humidity environment, something which has not been achieved before due to the sensitivity of the packing fraction of suspensions like cornstarch and water to temperature and humidity.

Transient measurements of stress relaxation over time revealed that DST fluids exhibit unexpected relaxation behavior in certain parameter regimes (Fig. 8). For $\phi_{eff} < 58.2 \pm 0.7\%$, we observed an exponential decay with timescale T_1 , which is consistent with a relaxation time scale T_N determined by a rheometric fluid model in which the viscosity as a function of shear rate $\eta(\dot{\gamma})$ in steady state also controls the transient relaxation.

However, for larger ϕ_{eff} , the measured relaxation time becomes distinct from T_N , and two distinct exponential relaxations with timescales T_1 and T_2 were observed for $\phi_{eff} \geq 59.7 \pm 0.7\%$. The discrepancy between the measured relaxation times and the rheometric prediction T_N was measured to be as large as 4 orders of magnitude and diverges in the limit as $\phi_{eff} \rightarrow \phi_c = 61.0 \pm 0.7\%$ (corresponding to the liquid solid transition) as the measured relaxation times diverge to infinity while T_N approaches 0. At this point it is unknown what causes these discrepancies.

A nonzero relaxation time in the limit of large packing fractions may have important consequences for the phenomena exhibited by DST fluids. For example, after an impacting object stops, if the relaxation followed a rheometric model, expected relaxation times would be in the millisecond range and faster. This would be far too short for a pool of cornstarch and water to support a load like a solid long enough for a person to step on it while they run across (a duration of typically 0.15 s) [18]. Other phenomena like the velocity oscillations of a sinking sphere [21] or rolling a sphere on the surface of the suspension [26] would end much too fast to be observable by the naked eye based on the rheometric model. For such phenomena to be noticeable as dynamic with the naked eye requires a timescale on the order of seconds, which is in the range of what we find a large packing fractions. How to specifically model such phenomena with a constitutive relation that includes a relaxation time, for example using the model of Ozgen et al. [19] is left open for future work.

Acknowledgments

We would like to thank Heinrich Jaeger for valuable discussions and suggestions. This work was supported by the National Science Foundation under grant DMR-1410157.

-
- [1] H. Barnes. Shear-thickening (“dilatancy”) in suspensions of nonaggregating solid particles dispersed in newtonian liquids. *J. Rheology*, 33(2):329, 1989.
 - [2] E. Bertrand, J. Bibette, and V. Schmitt. From shear thickening to shear-induced jamming. *Physical Review E*, 66(6):060401, 2002.
 - [3] J. Brady and J. Morris. Microstructure of strongly sheared suspensions and its impact on rheology and diffusion. *J. Fluid Mech.*, 348:103–139, 1997.
 - [4] E. Brown and H. Jaeger. Shear thickening in concentrated suspensions: phenomenology and mechanisms and relations to jamming. *Reports on Progress in Physics*, 77:046602–1–23, 2014.
 - [5] E. Brown and H. M. Jaeger. Dynamic jamming point for shear thickening suspensions. *Phys. Rev. Lett.*, 103:086001, 2009.
 - [6] E. Brown, H. Zhang, N. A. Forman, B. W. Maynor, D. E. Betts, J. M. DeSimone, , and H. M. Jaeger. Shear thickening and jamming in densely packed suspensions of different particle shapes. *Phys. Rev. E*, 84:031408–1–11, 2011.
 - [7] R. Deegan. Stress hysteresis as the cause of persistent holes in particulate suspensions. *Phys. Rev. E*, 81:036319, 2010.
 - [8] E. Brown and H. Jaeger. The role of dilation and confining stress in shear thickening of dense suspensions. *J. Rheology*, 56(4):875–923, 2012.
 - [9] M. D. Ediger, C. A. Angell, and S. R. Nagel. Supercooled liquids and glasses. *Journal of Physical Chemistry*, 100:13200–13212, 1996.

- [10] R. Farr, J. Melrose, and R. Ball. Kinetic theory of jamming in hard-sphere startup flows. *Phys. Rev. E*, 55(6):7203–7211, 1997.
- [11] <http://www.d3o.com/>. 2013.
- [12] Y. Lee, , and N. Wagner. Dynamic properties of shear thickening colloidal suspensions. *Rheol. Acta*, 42:199–208, 2003.
- [13] Y. Lee, E. Wetzel, and N. Wagner. The ballistic impact characteristics of kevlar-woven fabrics impregnated with a colloidal shear thickening fluid. *J. Materials Sci.*, 38:2825, 2003.
- [14] N. Y. C. Lin, B. M. Guy, M. Hermes, C. Ness, J. Sun, W. C. K. Poon, and I. Cohen. Hydrodynamic and contact contributions to shear thickening in colloidal suspensions. *Physical Review Letters*, 115:228304, 2015.
- [15] A. Liu and S. Nagel. Jamming is not just cool any more. *Nature*, 396:21, 1998.
- [16] F. Merkt, R. Deegan, D. Goldman, E. Rericha, and H. Swinney. Persistent holes in a fluid. *Phys. Rev. Lett.*, 92(18):184501, 2004.
- [17] J. Mewis and N. J. Wagner. *Colloidal Suspension Rheology*. Cambridge University Press, 2012.
- [18] S. Mukhopadhyay, B. Allen, and E. Brown. A shear thickening transition in concentrated suspensions under impact. *arXiv:140719.*, 2014.
- [19] O. Ozgen, E. Brown, and M. Kallman. Simulating the dynamic behavior of shear thickening fluids. *arXiv:1510.09069v1*, 2015.
- [20] S. Raghavan and S. Khan. Shear-thickening response of fumed silica suspensions under steady and oscillatory shear. *J. Colloid and Interface Science*, 185:57–67, 1997.
- [21] S. von Kann, J. H. Snoeijer, D. Lohse, and D. van der Meer. Non-monotonic settling of a sphere in a cornstarch suspension. *Phys. Rev. E*, 84:060401, 2011.
- [22] S. von Kann, J. H. Snoeijer, and D. van der Meer. Velocity oscillations and stop-go cycles: The trajectory of an object settling in a cornstarch suspension. *Phys. Rev. E*, 87:042301, 2013.
- [23] N. Wagner and J. Brady. Shear thickening in colloidal dispersions. *Phys. Today, Oct. 2009*, pages 27–32, 2009.
- [24] S. Waitukaitis and H. Jaeger. Impact-activated solidification of dense suspensions via dynamic jamming fronts. *Nature*, 487:205–209, 2012.
- [25] YouTube. *Search for 'Running on Cornstarch and Water'*, 2016.
- [26] YouTube. *Search for 'Bowling ball Cornstarch and Water'*, 2016.